ChemComm

COMMUNICATION

View Article Online
View Journal

Cite this: DOI: 10.1039/d6cc01367h

Received 6th March 2026,
Accepted 24th April 2026

DOI: 10.1039/d6cc01367h

rsc.li/chemcomm

Exploration of naphtho[c]dithiophenes: synthesis and optical and electrochemical properties of naphtho[1,2-*c*:5,6-*c*′]dithiophenes

Yuki Okazaki, Shogo Amimoto, Kumpei Kozuka, Satoru Maekawa, Keiichi Imato and Yousuke Ooyama *

An efficient synthetic method for naphtho[1,2-*c*:5,6-*c*′]dithiophenes and their tetrasubstituted derivatives has been developed and their photophysical and electrochemical properties were investigated. The naphtho[c]dithiophene skeleton as a new thiophene-fused polycyclic aromatic system can be used as a π-building block in emitters, semiconductors and photosensitizers for organic optoelectronic devices.

Thiophene-fused polycyclic aromatic systems are of scientific and practical interest in synthetic organic chemistry, photochemistry and electrochemistry, and serve as key constituents of emitters, semiconductors and photosensitizers for organic optoelectronic devices.[1–5] In particular, benzo[*b*]thiophenes and naphtho[*b*]dithiophenes, including naphtho[2,3-*b*:6,7-*b*′]dithiophene, naphtho[2,3-*b*:7,6-*b*′]dithiophene, naphtho[1,2-*b*:5,6-*b*′]dithiophene, and naphtho[2,1-*b*:6,5-*b*′]dithiophene, exhibiting high charge transport properties are widely used in organic field-effect transistors (OFETs), organic photovoltaics (OPVs), and organic light-emitting diodes (OLEDs) (Fig. 1a).[6–15] Meanwhile, benzo[*c*]thiophenes, 1,1′- and 4,4′-bibenzo[*c*]thiophenes and fused-bibenzo[*c*]thiophenes have received considerable attention in recent years not only due to the challenges in developing facile and efficient synthetic methods, but also due to their attractive photophysical and electrochemical properties, which make them promising fluorophores and photosensitizers for highly efficient bioimaging, phototheranostics, and optoelectronic devices (Fig. 1b).[16–30]

Inspired by the strategic research for the development and practical application of thiophene-fused polycyclic aromatic systems, which are attracting increasing attention, we devised a strategy to construct naphtho[*c*]dithiophenes and to investigate their photophysical and electrochemical properties. Herein, we report an efficient synthetic method for naphtho[1,2-*c*:5,6-*c*′]dithiophene (**N[*c*]DT-1**) and its tetrasubstituted derivative (**N[*c*]DT-Si4**) with four *tert*-butyldimethylsilyl groups on two thiophene rings (Fig. 1c) and investigate their photophysical and electrochemical properties using photoabsorption and fluorescence spectroscopies, cyclic voltammetry (CV), and density functional theory (DFT) calculations. It was found that **N[*c*]DT-1** exhibits intense vibronic-structured photoabsorption and fluorescence bands in the long-wavelength region and a high HOMO energy level and a low LUMO energy level, compared to its structural isomers naphtho[*b*]dithiophenes, naphtho[1,2-*b*:5,6-*b*′]dithiophene (**N[*b*]DT-3**) and naphtho[2,1-*b*:6,5-*b*′]dithiophene (**N[*b*]DT-4**) as well as isoelectronic chrysene with **N[*c*]DT-1**. Indeed, this work is the first to report the synthesis and photophysical and electrochemical characteristics of naphtho[*c*]dithiophenes.

N[*c*]DT-1 and its tetrasilyl-substituted derivative (**N[*c*]DT-Si4**) were synthesized according to a stepwise synthetic protocol (Scheme 1). The starting compound **1**, 1,2,5,6-tetramethylnaphthalene, was prepared through the Wolff–Kishner reduction of 2,6-dimethylnaphthalene-1,5-dicarbaldehyde, which was prepared through Bodroux–Chichibabin aldehyde synthesis using

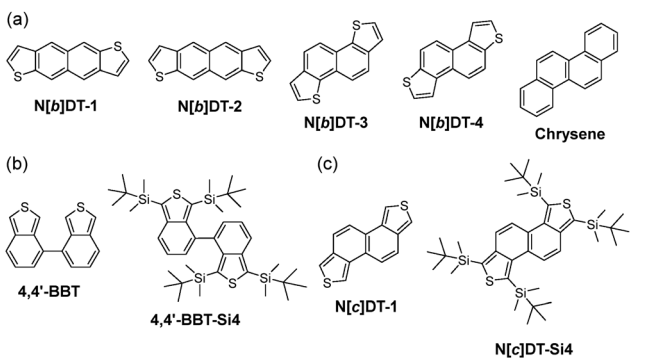

Fig. 1 (a) Chemical structures of naphtho[*b*]dithiophenes (ref. 10) and chrysene. (b) Previous work (ref. 25) for 4,4′-bibenzo[c]thiophenes and (c) this work for naphtho[c]dithiophenes.

Applied Chemistry Program, Graduate School of Advanced Science and Engineering, Hiroshima University, 1-4-1 Kagamiyama, Higashi-Hiroshima 739-8527, Japan. E-mail: yooyama@hiroshima-u.ac.jp

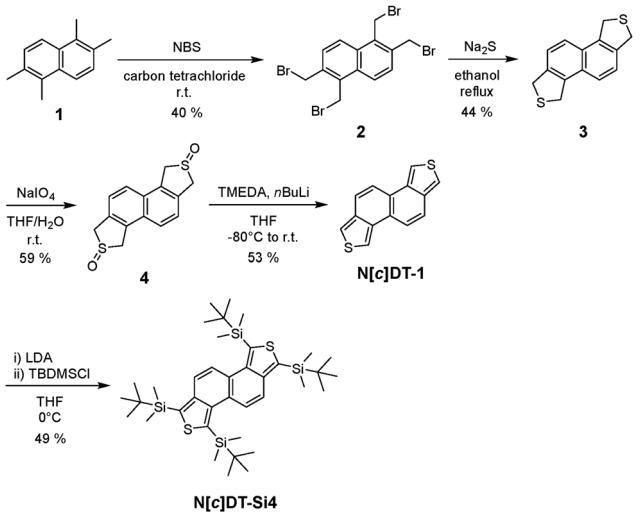

Scheme 1 Synthetic route to naphtho[1,2-*c*:5,6-*c*′]dithiophenes **N[*c*]DT-1** and **N[*c*]DT-Si4**.

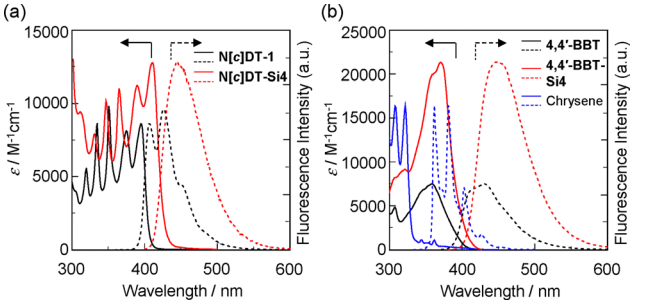

Fig. 2 Photoabsorption (solid line) and fluorescence (dotted line) spectra of (a) **N[*c*]DT-1** (1.0×10^{-4} M) and **N[*c*]DT-Si4** (5.0×10^{-5} M), (b) **4,4′-BBT** (3.0×10^{-5} M), **4,4′-BBT-Si4** (3.0×10^{-5} M), and chrysene (5.0×10^{-5} M) in toluene. Fluorescence intensity is normalized.

1,5-dibromo-2,6-dimethylnaphthalene (Scheme S1, SI), because commercially available compound **1** is very expensive. The bromination of **1** with *N*-bromosuccinimide (NBS) gave compound **2** with a yield of 40%. Tetrahydronaphtho[1,2-*c*:5,6-*c*′]dithiophene **3** was obtained in a yield of 44% by the reaction of **2** with sodium sulfide. The oxidation of **3** with sodium periodate gave sulfoxide **4** with a moderate yield (59%), which is a key intermediate in the synthesis of naphtho[1,2-*c*:5,6-*c*′]dithiophenes. Indeed, naphtho[1,2-*c*:5,6-*c*′]dithiophene (**N[*c*]DT-1**) was successfully prepared in a yield of 53% or 30% by treatment of **4** with tetramethylethylenediamine (TMEDA) and then *n*BuLi or with lithium hexamethyldisilazide (LHMDS) (see the SI). Furthermore, the tetrasilyl-substituted derivative (**N[*c*]DT-Si4**) was obtained in a yield of 49% by the reaction of **N[*c*]DT-1** with lithium diisopropylamide (LDA), followed by treatment with *tert*-butyldimethylsilyl chloride (TBDMSCl) as an electrophile. **N[*c*]DT-1** and **N[*c*]DT-Si4** were successfully characterized by FTIR, ^{1}H and ^{13}C NMR measurements and HRMS analysis. Therefore, this result proposes a facile and stepwise synthetic method for the introduction of various substituents, including bromo, stannyl, and boronic acid functional groups for the Stille or Suzuki coupling reaction, into the thiophene rings of the naphtho[1,2-*c*:5,6-*c*′]dithiophene skeleton.

The photoabsorption and fluorescence spectra of **N[*c*]DT-1** and **N[*c*]DT-Si4**, **4,4′-BBT** and **4,4′-BBT-Si4** as non-fused bibenzo[*c*]thiophenes, and isoelectronic chrysene with **N[*c*]DT-1** in toluene are shown in Fig. 2, and their photophysical data along with those of **N[*b*]DT-3** and **N[*b*]DT-4** are summarized in Table 1. **N[*c*]DT-1** and **N[*c*]DT-Si4** exhibit vibronic-structured photoabsorption bands similar to **N[*b*]DT-3**, **N[*b*]DT-4** and chrysene, although **4,4′-BBT** and **4,4′-BBT-Si4** exhibit broad photoabsorption bands. The photoabsorption maximum wavelength (λ_{max}^{abs} = 395 nm) of **N[*c*]DT-1** showed bathochromic shifts by 36 nm, 75 nm, 45 nm and 73 nm, compared to those of **4,4′-BBT**, **N[*b*]DT-3**, **N[*b*]DT-4** and chrysene, respectively. Furthermore, similar to **4,4′-BBT** and **4,4′-BBT-Si4**, **N[*c*]DT-Si4** exhibits an intense photoabsorption band (λ_{max}^{abs} = 411 nm) with a relatively high molar absorption coefficient (ε_{max} = 12 700 M^{-1} cm^{-1}) at a longer wavelength by 16 nm, compared to **N[*c*]DT-1** (ε_{max} = 8600 M^{-1} cm^{-1}). The corresponding fluorescence band of **N[*c*]DT-1** has a vibrational structure, similar to that of chrysene, while that of **N[*c*]DT-Si4** is broadened, similar to those of **4,4′-BBT** and **4,4′-BBT-Si4** (Fig. 2). It is worth noting here that the fluorescence maximum wavelength (λ_{max}^{fl} = 407 nm) of **N[*c*]DT-1** appeared at a shorter wavelength by 38 nm, 3 nm and 44 nm, respectively, compared to those (445 nm, 410 nm and 451 nm, respectively) of **N[*c*]DT-Si4**, **4,4′-BBT** and **4,4′-BBT-Si4**. Thus, the Stokes shift (7.46×10^{2} cm^{-1}) of **N[*c*]DT-1** is significantly smaller than those (1.85×10^{3} cm^{-1}, 3.46×10^{3} cm^{-1}, 4.78×10^{3} cm^{-1}, and 3.43×10^{3} cm^{-1}, respectively) of **N[*c*]DT-Si4**, **4,4′-BBT**, **4,4′-BBT-Si4**, and chrysene. Obviously, this result indicates that **N[*c*]DT-1** has a rigid and expanded π-conjugation structure, compared to **4,4′-BBT**. Meanwhile, for **N[*c*]DT-Si4**, the broad fluorescence band and a relatively large Stokes shift (SS) value are due to the rotatable and flexible *tert*-butyldimethylsilyl group. However, the fluorescence quantum yield (Φ_{fl} = 0.20) of **N[*c*]DT-1** is higher than those (0.10) of **N[*c*]DT-Si4** and chrysene, but is lower than those (0.41 and 0.36, respectively) of **4,4′-BBT** and **4,4′-BBT-Si4**. Time-resolved fluorescence spectroscopy demonstrated that the fluorescence lifetimes (τ_{fl} = 2.93 ns and 1.00 ns) of **N[*c*]DT-1** and **N[*c*]DT-Si4** are a little shorter than those (3.46 ns and 3.59 ns) of **4,4′-BBT** and **4,4′-BBT-Si4**, but much shorter than that (12.1 ns) of chrysene. The radiative rate constant ($k_r = 6.8 \times 10^{7}$ s^{-1}) for **N[*c*]DT-1** is about one-half those ($1.0–1.1 \times 10^{8}$ s^{-1}) for **N[*c*]DT-Si4**, **4,4′-BBT** and **4,4′-BBT-Si4**, but the k_r value (8.2×10^{6} s^{-1}) for chrysene is much smaller than those for the other four compounds. In contrast, the nonradiative rate constant ($k_{nr} = 9.0 \times 10^{8}$ s^{-1}) for **N[*c*]DT-Si4** is significantly larger than those ($7.4 \times 10^{7}–2.7 \times 10^{8}$ s^{-1}) for the other four compounds. Thus, the ratio (k_{nr}/k_r = 9.0) of the nonradiative constant to the radiative constant for **N[*c*]DT-Si4** and chrysene is larger than those (4.0, 1.5 and 1.7, respectively) for **N[*c*]DT-1**, **4,4′-BBT** and **4,4′-BBT-Si4**, indicating that the lower Φ_{fl} values of **N[*c*]DT-Si4** and chrysene are mainly due to the larger k_{nr} value and smaller k_r value, respectively, compared to the Φ_{fl} values of **N[*c*]DT-Si4**, **4,4′-BBT** and **4,4′-BBT-Si4**. Consequently, these facts for the naphtho[1,2-*c*:5,6-*c*′]dithiophene skeleton compared to the 4,4′-bibenzo[*c*]thiophene skeleton, that is, the vibronic-structured

Table 1 Photophysical and electrochemical data and HOMO and LUMO energy levels of naphtho[*c*]dithiophenes, 4,4′-bibenzo[*c*]thiophenes, naphtho[*b*]dithiophenes, and chrysene in the solution

Dye	λ_{max}^{abs}/nm (ε_{max}/M^{-1} cm^{-1})	λ_{max}^{fl}/nm (Φ_{fl})[f]	SS/cm^{-1}	τ_{fl}[g]/ns	k_r[h]/s^{-1}	k_{nr}[i]/s^{-1}	k_{nr}/k_r	E_{onset}^{ox}[j]/V	E_g^{opt}[k]/eV	HOMO[l]/eV	LUMO[l]/eV
N[*c*]DT-1	395[c] (8600)[a]	407[d] (0.20)[a]	7.46×10^2	2.93[a]	6.8×10^{7a}	2.7×10^{8a}	4.0[a]	0.50	3.10[a]	−5.30	−2.20
N[*c*]DT-Si4	411[c] (12 700)[a]	445 (0.10)[a]	1.85×10^3	1.00[a]	1.0×10^{8a}	9.0×10^{8a}	9.0[a]	0.59	2.94[a]	−5.39	−2.45
4,4′-BBT[m]	359 (7500)[a]	410 (0.41)[a]	3.46×10^3	3.46[a]	1.1×10^{8a}	1.7×10^{8a}	1.5[a]	0.75[m]	3.16[a]	−5.55	−2.39
4,4′-BBT-Si4[m]	371 (21 300)[a]	451 (0.36)[a]	4.78×10^3	3.59[a]	1.0×10^{8a}	1.7×10^{8a}	1.7[a]	0.54[m]	3.04[a]	−5.34	−2.30
N[*b*]DT-3[n]	320[e] (—[o])[b]	—[o]	—[o]	—[o]	—[o]	—[o]	—[o]	—[o]	3.90[b]	−5.80	−1.90
N[*b*]DT-4[n]	350[e] (—[o])[b]	—[o]	—[o]	—[o]	—[o]	—[o]	—[o]	—[o]	3.50[b]	−5.70	−2.20
Chrysene	322[c] (16 400)[a]	362[d] (0.10)[a]	3.43×10^3	12.1[a]	8.2×10^{6a}	7.4×10^{7a}	9.0[a]	1.00[p]	3.71[a]	−5.80	−2.09

[a] In toluene. [b] In dichloromethane. [c] The longest wavelength maximum of the vibronic-structured photoabsorption band. [d] The shortest wavelength maximum of the vibronic-structured fluorescence band. [e] Photoabsorption edge. [f] Fluorescence quantum yields (Φ_{fl}) were determined by using a calibrated integrating sphere system (λ^{ex} = 366 nm, 366 nm, 359 nm, 371 nm, and 318 nm for **N[*c*]DT-1**, **N[*c*]DT-Si4**, **4,4′-BBT**, **4,4′-BBT-Si4**, and chrysene, respectively). [g] Fluorescence lifetime. [h] Radiative rate constant ($k_r = \Phi_{fl}/\tau_{fl}$). [i] Nonradiative rate constant ($k_{nr} = (1 - \Phi_{fl})/\tau_{fl}$). [j] Onset potentials (E_{onset}^{ox}) *versus* Fc/Fc$^+$ of the oxidation potential. [k] Optical energy gaps (E_g^{opt}) of **N[*c*]DT-1**, **N[*c*]DT-Si4**, **4,4′-BBT**, and **4,4′-BBT-Si4** were determined from the intersection (400 nm, 422 nm, 393 nm, and 408 nm, respectively) of photoabsorption and fluorescence spectra in toluene. E_g^{opt} values of **N[*b*]DT-3**, **N[*b*]DT-4**, and chrysene were determined from the photoabsorption edge (320 nm, 350 nm, and 334 respectively). [l] *Versus* the vacuum level. [m] Previous work (ref. 25). [n] Ref. 10. [o] No data. [p] See Fig. S22 for the cyclic voltammogram, SI.

photoabsorption and fluorescence bands in the long-wavelength region, the mirror symmetry relationship, and the small Stokes shift value indicate that naphtho[*c*]dithiophene has a rigid and expanded π-conjugation structure.

The electrochemical properties of **N[*c*]DT-1** and **N[*c*]DT-Si4** were determined using CV in DMF containing 0.1 M tetrabutylammonium perchlorate (Bu_4NClO_4). The potentials were internally referenced to ferrocene/ferrocenium (Fc/Fc$^+$). The cyclic voltammograms of the two compounds are shown in Fig. 3, and their electrochemical data and the HOMO and LUMO energy levels are summarized in Table 1. The irreversible oxidation wave was observed at 0.68 V for **N[*c*]DT-1** and 0.76 V for **N[*c*]DT-Si4**, while any obvious reduction wave did not appear within the potential window (−1.5 V to 0 V *versus* Fc/Fc$^+$). Thus, the oxidation wave for **N[*c*]DT-1** is slightly cathodically shifted by *ca.* 0.10 V, compared to that for **N[*c*]DT-Si4**. The HOMO energy levels (−[E_{onset}^{ox} + 4.8] eV) *versus* the vacuum level were estimated from the onset potentials (E_{onset}^{ox} = 0.50 V for **N[*c*]DT-1** and 0.59 V for **N[*c*]DT-Si4**) of the oxidation waves, and the LUMO energy levels were estimated from the E_{onset}^{ox} and intersections (optical energy gap: E_g^{opt} = 3.10 eV for **N[*c*]DT-1** and 2.94 eV for **N[*c*]DT-Si4**) of the photoabsorption and fluorescence spectra in toluene. The HOMO energy level (−5.30 eV) of **N[*c*]DT-1** is significantly higher than those (−5.55 eV, −5.80 eV, −5.70 eV, and −5.80 eV) of **4,4′-BBT**, **N[*b*]DT-3**, **N[*b*]DT-4** and chrysene. Meanwhile, the LUMO energy level (−2.20 eV) of **N[*c*]DT-1** is equivalent to that of **N[*b*]DT-4**, but is lower than those (−1.90 eV and −2.09 V) of **N[*b*]DT-3** and chrysene and is somewhat higher than that (−2.39 eV) of **4,4′-BBT**. Consequently, it was revealed that the bathochromic shift of the photoabsorption band for **N[*c*]DT-1** relative to **4,4′-BBT**, **N[*b*]DT-3**, **N[*b*]DT-4** and chrysene is attributed not only to destabilization of the HOMO energy level but also to stabilization of the LUMO energy level due to the naphtho[*c*]dithiophene skeleton, resulting in a decrease in the HOMO–LUMO band gap. Interestingly, the HOMO and LUMO energy levels of **N[*c*]DT-Si4** are lower than those of **N[*c*]DT-1**, but the lowering of the LUMO energy level is larger than that of the HOMO energy level, whereas the HOMO and LUMO energy levels of **4,4′-BBT-Si4** are higher that those of **4,4′-BBT**, but the rise of the HOMO energy level is larger than that of the LUMO energy level, resulting in a decrease in the HOMO–LUMO band gap, that is, a bathochromic shift of the photoabsorption band.

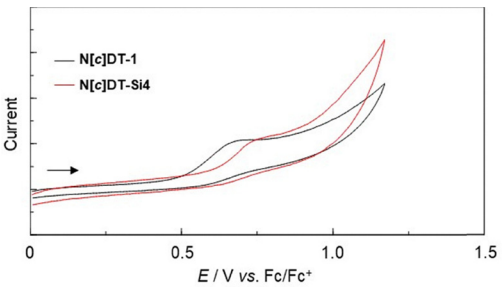

Fig. 3 Cyclic voltammograms of **N[c]DT-1** and **N[c]DT-Si4** in DMF containing 0.1 M Bu_4NClO_4 at a scan rate of 100 mV s^{-1}. The arrow denotes the direction of the potential scan.

To examine the electronic structures of naphtho[1,2-*c*:5,6-*c*′]dithiophenes, the molecular orbitals of **N[*c*]DT-1** and **N[*c*]DT-Si4** were calculated using DFT at the B3LYP/6-31G(d,p) level (Fig. S23). Similar to chrysene, the HOMO and the LUMO of **N[*c*]DT-1** and **N[*c*]DT-Si4** are delocalized over the whole molecule. The DFT calculations demonstrated that the HOMO and LUMO energy levels of **N[*c*]DT-1** are higher and lower than those of **4,4′-BBT**, **N[*b*]DT-3**, **N[*b*]DT-4** and chrysene, respectively, similar to the experimental results, resulting in a decrease in the HOMO–LUMO band gap. The fact that the HOMO–LUMO band gaps of **N[*b*]DT-3**, **N[*b*]DT-4** and chrysene are wider than that of **N[*c*]DT-1** can be understood from Clar's aromatic π-sextet rule, which states that the HOMO–LUMO band gap widens as the number of aromatic π-sextet in polycyclic aromatic hydrocarbon increases; **N[*b*]DT-3**, **N[*b*]DT-4** and chrysene have four aromatic π-sextets, while **N[*c*]DT-1** has two aromatic π-sextets.[31] In addition, as in the case of **4,4′-BBT** and **4,4′-BBT-Si4**, the LUMO energy level of **N[*c*]DT-Si4** is similar to that of **N[*c*]DT-1**, whereas the HOMO energy level of **N[*c*]DT-Si4**

is higher than that of **N[*c*]DT-1**, leading to a decrease in the HOMO–LUMO band gap. This result suggests that the destabilization of the HOMO energy level is due to the introduction of the electron-donating *tert*-butyldimethylsilyl group into the thiophene ring, although the change in the HOMO energy level from **N[*c*]DT-1** to **N[*c*]DT-Si4** according to the DFT calculations is opposite to the experimental results. Furthermore, the time-dependent density functional theory (TD-DFT) calculations were performed to elucidate the photophysical properties of naphtho[1,2-*c*:5,6-*c*′]dithiophenes (Fig. S24). The calculated $\lambda_{max}^{abs\text{-}calcd}$ of the seven compounds appears in longer wavelength regions in the order of **N[*b*]DT-3** (308 nm) < **N[*b*]DT-4** (317 nm) ≈ chrysene (322 nm) < **4,4′-BBT** (345 nm) < **4,4′-BBT-Si4** (356 nm) < **N[*c*]DT-1** (402 nm) < **N[*c*]DT-Si4** (428 nm), and the calculated ε_{calcd} increases in the order of **N[*c*]DT-1** (4200 M^{-1} cm^{-1}) < chrysene (5300 M^{-1} cm^{-1}) < **N[*b*]DT-3** (6100 M^{-1} cm^{-1}) < **N[*c*]DT-Si4** (6700 M^{-1} cm^{-1}) < **4,4′-BBT** (7800 M^{-1} cm^{-1}) < **N[*b*]DT-4** (12 200 M^{-1} cm^{-1}) < **4,4′-BBT-Si4** (15 600 M^{-1} cm^{-1}). The $S_0 \rightarrow S_1$ transitions are mainly attributed to the transitions from the HOMO to the LUMO (99% for **N[*c*]DT-1**, 99% for **N[*c*]DT-Si4**, 67% for **4,4′-BBT**, 68% for **4,4′-BBT-Si4**, 55% for **N[*b*]DT-3**, and 89% for **N[*b*]DT-4**, 52% for chrysene). Indeed, the TD-DFT calculations are in good agreement with the experimental results regarding the bathochromic shift of the photoabsorption band from **N[*b*]DT-3** to **N[*c*]DT-Si4**, although there are differences in the ε_{calcd} values between the experimental and TD-DFT calculation results.

In conclusion, in order to construct naphtho[*c*]dithiophenes and to investigate their optical and electrochemical properties, we developed an efficient synthetic method for naphtho[1,2-*c*:5,6-*c*′]dithiophene (**N[*c*]DT-1**) and its tetrasubstituted derivative (**N[*c*]DT-Si4**) with four *tert*-butyldimethylsilyl groups on two thiophene rings for the first time. Furthermore, this facile synthetic method will allow the introduction of various substituents, including bromo, stannyl, and boronic acid functional groups for the Stille or Suzuki coupling reaction, into the thiophene rings of the naphtho[1,2-*c*:5,6-*c*′]dithiophene skeleton. The photophysical and electrochemical measurement, and density functional theory calculations revealed that naphtho[1,2-*c*:5,6-*c*′]dithiophenes possess intense vibronic-structured photoabsorption and fluorescence bands in the long-wavelength region and a high HOMO energy level and a low LUMO energy level, compared to their structural isomers naphtho[*b*]dithiophenes, naphtho[1,2-*b*:5,6-*b*′]dithiophene and naphtho[2,1-*b*:6,5-*b*′]dithiophene as well as isoelectronic chrysene with naphtho[1,2-*c*:5,6-*c*′]dithiophenes. Consequently, this work demonstrates that the naphtho[1,2-*c*:5,6-*c*′]dithiophene skeleton with the above advantageous properties would be used as a π-building block in emitters, semiconductors and photosensitizers for organic optoelectronic devices, and thus will open up research and development of new thiophene-fused polycyclic aromatic systems.

Prof. Yousuke Ooyama conceived the project. Dr Keiichi Imato directed the experimental work. Yuki Okazaki performed most of the experiments. Shogo Amimoto, Kumpei Kozuka, and Satoru Maekawa assisted with the experiment. The manuscript was written with contributions from all authors.

Conflicts of interest

The authors declare that there are no conflicts of interest.

Data availability

The data that support the findings of this work are available in the supplementary information (SI). Supplementary information: details of the experimental methods, and additional figures and tables. See DOI: https://doi.org/10.1039/d6cc01367h.

Acknowledgements

This work was supported by the Japan Society for the Promotion of Science (JSPS) KAKENHI Grant Numbers 25K01808 and 25K22857.

References

1 L. Guo, L. Wu, T. Jia, H. Zhang, J. Song, X. Xie, M. H. Jee, H. Ma, S. Liu, G. Lu, H. Y. Woo, Z. Wang, F. Gao and Y. Sun, *Angew. Chem., Int. Ed.*, 2025, **64**, e202516421.
2 D. Zhang, X. Zheng, Y. Zhao, C. Zhao, F. Huang and Y. He, *J. Phys. Chem. C*, 2024, **128**, 7377–7387.
3 D. Lee, J. Moon, S. Kim and J. Y. Lee, *Adv. Mater.*, 2026, e21668.
4 E. B. A. Adusei, S. Ibrahim, K. Jenneker, C. D. Goldsmith, D. Dragoi, M. Zeller and Z. J. Kinney, *J. Org. Chem.*, 2026, **91**, 394–400.
5 K. Kawabata, K. Mashimo and K. Takimiya, *Chem. Mater.*, 2024, **36**, 11920–11933.
6 K. Haase, J. P. Andrade, M. Hambsch, V. Sethumadhavan, W. He, T. Michinobu, P. Sonar and S. C. B. Mannsfeld, *Adv. Electron. Mater.*, 2025, **11**, e00375.
7 I. Osaka, T. Kakara, N. Takemura, T. Koganezawa and K. Takimiya, *J. Am. Chem. Soc.*, 2013, **135**, 8834–8837.
8 I. Osaka, T. Abe, S. Shinamura and K. Takimiya, *J. Am. Chem. Soc.*, 2011, **133**, 6852–6860.
9 S. Shinamura, E. Miyazaki and K. Takimiya, *J. Org. Chem.*, 2010, **75**, 1228–1234.
10 S. Shinamura, I. Osaka, E. Miyazaki, A. Nakao, M. Yamagishi, J. Takeya and K. Takimiya, *J. Am. Chem. Soc.*, 2011, **133**, 5024–5035.
11 M. E. Cinar and T. Ozturk, *Chem. Rev.*, 2015, **115**, 3036–3140.
12 J. Y. Kim, D. Yokoyama and C. Adachi, *J. Phys. Chem. C*, 2012, **116**, 8699–8706.
13 H. Usta, D. Kim, R. Ozdemir, Y. Zorlu, S. Kim, M. C. R. Delgado, A. Harbuzaru, S. Kim, G. Demirel, J. Hong, Y.-G. Ha, K. Cho, A. Facchetti and M.-G. Kim, *Chem. Mater.*, 2019, **31**, 5254–5263.
14 H. Tan, H. Tan, X. Zheng, J. Yang, J. Yu and W. Zhu, *J. Mater. Chem. C*, 2020, **8**, 3183–3191.
15 M. Liang and J. Chen, *Chem. Soc. Rev.*, 2013, **42**, 3453–3488.
16 P. Amaladass, R. Dhanusuraman, A. Lazer, D. John, K. Thangaraju and V. Dhayalan, *Asian J. Org. Chem.*, 2025, **14**, e202500085.
17 Y. Ooyama and K. Imato, *Tetrahedron Lett.*, 2025, **155**, 155393.
18 K.-W. Lee, Y. Cao, W.-C. Wei, J.-H. Tan, Y. Wan, Z. Feng, Y. Zhang, Y. Liu, X. Zheng, C. Cao, H. Chen, P. Wang, S. Li, K.-T. Wong and C.-S. Lee, *Adv. Mater.*, 2023, **35**, 2211632.
19 D. Yan, M. Wang, Q. Wu, N. Niu, M. Li, R. Song, J. Rao, M. Kang, Z. Zhang, F. Zhou, D. Wang and B. Z. Tang, *Angew. Chem., Int. Ed.*, 2022, **61**, e202202614.
20 D. Yan, W. Xie, J. Zhang, L. Wang, D. Wang and B. Z. Tang, *Angew. Chem., Int. Ed.*, 2021, **60**, 26769–26776.
21 Y. Wan, G. Lu, W.-C. Wei, Y.-H. Huang, S. Le, J.-X. Chen, X. Cui, Y.-F. Xio, X. Li, Y. Liu, X.-M. Meng, P. Wang, H.-Y. Xie, J. Zhang, K.-T. Wong and C.-S. Lee, *ACS Nano*, 2020, **14**, 9917–9928.
22 X. Chen, D. Zhang, Y. He, M. U. Ali, Y. Wu, C. Zhao, P. Wu, C. Yan, F. Wudl and H. Meng, *Mater. Chem. Front.*, 2020, **4**, 3578–3584.

23 K. Yamamoto, Y. Ie, M. Nitani, N. Tohnai, F. Kakiuchi, K. Zhang, W. Pisula, K. Asadi, P. W. M. Blom and Y. Aso, *J. Mater. Chem. C*, 2018, **6**, 7493–7500.
24 Y.-C. Hu, Z.-L. Lin, T.-C. Huang, J.-W. Lee, W.-C. Wei, T.-Y. Ko, C.-Y. Lo, D.-G. Chen, P.-T. Chou, W.-Y. Hung and K.-T. Wong, *Mater. Chem. Front.*, 2020, **4**, 2029–2039.
25 K. Obayashi, K. Imato, S. Aoyama, T. Enoki, S. Akiyama, M. Ishida, S. Suga, K. Mitsudo and Y. Ooyama, *RSC Adv.*, 2021, **11**, 18870–18880.
26 Y. Hara, K. Kozuka, K. Imato, S. Akiyama, M. Ishida and Y. Ooyama, *New J. Chem.*, 2024, **48**, 9890–9898.
27 T. Higashino, Y. Hara, K. Imato, S. Akiyama, M. Ishida and Y. Ooyama, *New J. Chem.*, 2023, **47**, 9555–9559.
28 K. Obayashi, S. Miho, M. Yasui, K. Imato, S. Akiyama, M. Ishida and Y. Ooyama, *New J. Chem.*, 2021, **45**, 17085–17094.
29 K. Obayashi, T. Higashino, K. Imato and Y. Ooyama, *New J. Chem.*, 2021, **45**, 13258–13261.
30 Y. Ooyama, T. Enoki, S. Aoyama and J. Ohshita, *Org. Biomol. Chem.*, 2017, **15**, 7302–7307.
31 E. Clar, *The Aromatic Sextet*, John Wiley & Sons, 1972.